Holocene climate and glacier variability at Hallet and Greyling Lakes, Chugach Mountains, south-central Alaska

Nicholas P. McKay · Darrell S. Kaufman

Abstract Evidence from lake sediments and glacier forefields from two hydrologically isolated lake basins is used to reconstruct Holocene glacier and climate history at Hallet and Greyling Lakes in the central Chugach Mountains of south-central Alaska. Glacial landform mapping, lichenometry, and equilibrium-line altitude reconstructions, along with changes in sedimentary biogenic-silica content, bulk density, and grain-size distribution indicate a dynamic history of Holocene climate variability. The evidence suggests a warm early Holocene from 10 to 6 ka, followed by the onset of Neoglaciation in the two drainage basins, beginning between 4.5 and 4.0 ka. During the past 2 ka, the glacial landforms and lacustrine sediments from the two valleys record a remarkably similar history of glaciation, with two primary advances, one during the first millennium AD, from ∼500 to 800 AD, and the second during the Little Ice Age (LIA) from ∼1400 to 1900 AD. During the LIA, the reconstructed equilibrium-line altitude in the region was no more than 83 ± 44 m ($n = 21$) lower than the modern, which is based on the extent of glaciers during 1978. Differences between the summer temperature inferred from the biogenic-silica content and the evidence for glacial advances and retreats suggest a period of increased winter precipitation from 1300 to 1500 AD, and reduced winter precipitation from 1800 to 1900 AD, likely associated with variability in the strength of the Aleutian Low.

Keywords Holocene climate change · Glaciolacustrine sediment · Aleutian Low · North Pacific, Alaska

This is one of fourteen papers published in a special issue dedicated to reconstructing late Holocene climate change from Arctic lake sediments. The special issue is a contribution to the International Polar Year and was edited by Darrell Kaufman.

N. P. McKay · D. S. Kaufman (✉)
Department of Geology, Northern Arizona University, Flagstaff, AZ 86011, USA
e-mail: Darrell.Kaufman@nau.edu

Present Address:
N. P. McKay
Department of Geosciences, University of Arizona, Tucson, AZ 85721, USA

Introduction

Because all paleoclimatic indicators are imperfect approximations of reality, a multiproxy approach to climate reconstruction is needed to overcome the inherent limitations of individual proxies (e.g., Osborn et al. 2007). This study focuses on the sedimentological and biological characteristics of sediment deposited in two glacier-fed lakes, in conjunction with the glacial history of their catchments. In addition to a combined terrestrial-lacustrine approach, by studying two nearby, but hydrologically isolated lakes that experience the same regional

climatic phenomena, but unique microclimates, we can better distinguish the effects of regional from local climate variability.

Although several studies have used lacustrine sediment records to infer Holocene climate variability in southern Alaska, few high-resolution (e.g., Loso et al. 2006; Loso this volume) or quantitative estimates (e.g., Hu et al. 2001; McKay et al. 2008) that extend through the past 2 ka have been developed for the region. The glacial history of the past 2 ka in southern Alaska is better known; evidence from the forefields of numerous glaciers in the Wrangell, St. Elias, Kenai, and Chugach mountain ranges was recently summarized by Wiles et al. (2008). Previous multiproxy, glacier-lake investigations have been reported for south Alaska (e.g., Levy et al. 2004; Daigle and Kaufman 2008), but these are relatively low-resolution records. Here, we use glacial-landform mapping, lichenometry, and equilibrium-line altitude reconstructions, along with changes in sedimentary biogenic-silica content, bulk density, organic-matter content, grain-size distribution and sedimentation rate to develop a high-resolution record of regional climate for the past 2 ka, and a lower-resolution record for the entire Holocene.

Study area

Hallet and Greyling Lakes are located along the crest of the northeastern Chugach Mountains, about 50 km north of Valdez and within the drainage of the Copper River (Fig. 1). The lakes were chosen for this study because they are among the few in the region accessible by floatplane, and because they afford an opportunity for a paired-lake study of relatively similar glacier-fed systems.

Hallet and Greyling Lakes are situated in a transitional climate regime between the maritime region of Prince William Sound to the south and the continental regime of interior Alaska to the north (Papineau 2001). Winter atmospheric circulation in the region is dominated by the Aleutian Low-pressure system, a regional-scale low-pressure center that is most developed during the winter. The strength and position of the Aleutian Low control winter temperature and precipitation, whereby a deepened Aleutian Low corresponds to warmer and wetter winters in south-central Alaska (Rodionov et al. 2005).
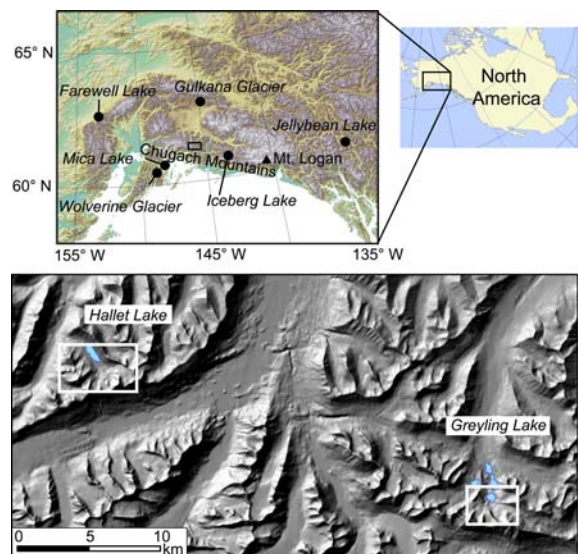

Fig. 1 Study area in the northeast Chugach Range, south-central Alaska. Area of the shaded relief map is shown as the black rectangle in regional map. Locations of other proxy climate records include: Farewell Lake (Hu et al. 2001), Iceberg Lake (Loso et al. 2006; Loso this volume), Mica Lake (Schiff et al. this volume), Jellybean Lake (Anderson et al. 2005) and Mt. Logan/Eclipse ice field (Fisher et al. 2004). Long-term glacier mass-balance records include: Wolverine and Gulkana Glaciers (Dyurgerov et al. 2002). White rectangles are map areas shown in Fig. 3
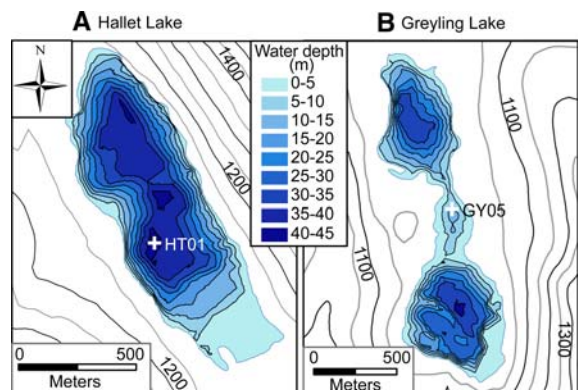

Fig. 2 Bathymetric maps of (**a**) Hallet Lake, and (**b**) Greyling Lake. Core sites for this study are indicated by white crosses. Topographic contours in m asl

Hallet Lake (61.5° N, 146.2° W, 1128 m asl) occupies a glacial valley dammed by debris avalanches (Fig. 2). The lake covers 0.6 km², and has relatively simple bathymetry, with fan deltas located at the mouths of the two major inflows, and an otherwise flat lake bottom, 41 m deep at its deepest

point (Fig. 2a). The drainage basin is 9.4 km^2, including seven cirque glaciers that range from 0.1 to 0.7 km^2, based on aerial photographs taken in 1978.

Greyling Lake (61.4° N, 145.7° W) is located 30 km east of Hallet Lake, also near the crest of the range at 1015 m asl. The lake is elongate, approximately 2 km long, with three distinct sub-basins (Fig. 2b). It covers 0.7 km^2, is 36 m deep at its deepest point, and its drainage area covers 10 km^2, including four cirque glaciers that range from 0.3 to 1 km^2. Greyling Lake is fed by the outlet of Upper Greyling Lake (informal name), which is located about 0.3 km up valley.

Methods

Glacial history

Glacial landform mapping and lichenometry

The series of prominent late Holocene moraines formed in the forefields of extant glaciers at the head of both Greyling and Hallet Lake valleys were mapped during July 2006. Twenty-six lichen stations (13 in each valley) were established on clearly defined moraines (Fig. 3) to estimate the timing of the multiple moraine-forming intervals. The age of each landform was calculated by applying the length of the long axis of the largest, approximately circular *Rhizocarpon* lichen to an empirically derived growth curve; if the largest lichen was >20% larger than the second largest, then it was assumed to be inherited from an older surface and was rejected. Because a lichen growth curve has not yet been developed for the Chugach Range, we relied on the existing curve for the Wrangell–St. Elias Mountains, which was recently updated by Solomina and Calkin (2003), and is also based on the single-largest circular lichen:

$$t = -1018.4 + 30.095D \text{ (linear phase)} \quad (1)$$

$$t = 38.813 \times 10^{(0.022408D)} \text{ (great period)} \quad (2)$$

where t = age in years before the measurement (2006 AD), and D = lichen diameter in mm. Equation (2) represents the initial phase of non-linear growth, which encompasses the interval of most lichen ages measured in the field area. The age uncertainty is estimated to be ±20% (Solomina and Calkin 2003).
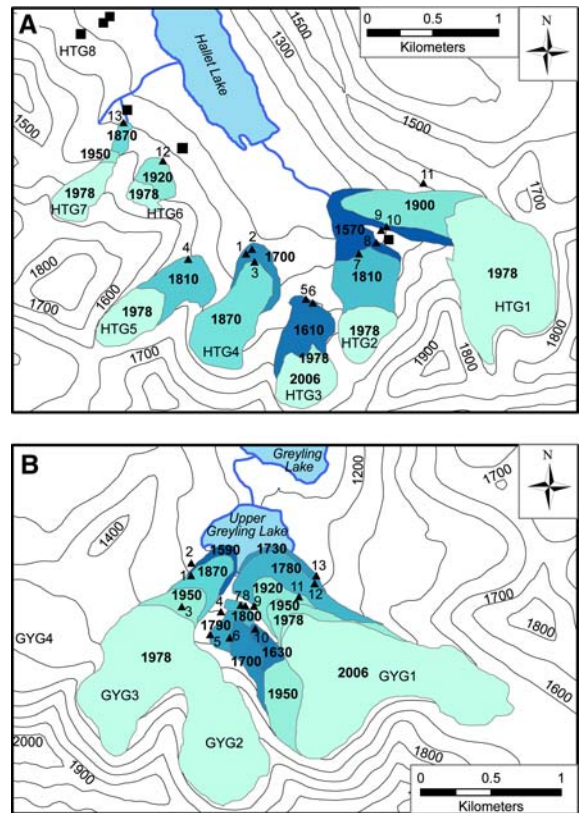

Fig. 3 Reconstructed glacier extents during the past 500 years in the headwaters of (**a**) Hallet Lake, and (**b**) Greyling Lake. Four-digit numbers = ages in year AD. Ice extents were delimited based on: 2006 = field mapping; 1978 = 1:63,360-scale aerial photographs; 1950 = USGS topographic maps; all others = glacial moraines and lichenometric ages. Black triangles = lichen stations (data listed in Table 1). Black squares = landforms with lichens older than the Little Ice Age. Contour intervals in m asl. Map areas shown in Fig. 1

Equilibrium-line altitudes

The accumulation area ratio (AAR) method (Meier and Post 1962) was used to estimate the equilibrium-line altitudes (ELA) for 25 "modern" glaciers (16 near Greyling Lake and nine near Hallet Lake) in the study area, and to reconstruct the ELA for the maximum LIA ice extent of each glacier. The reconstructed ELAs were used to estimate ELA lowering (ΔELA) (the difference between the ELA for "modern" and the ELA reconstructed for the LIA) for each glacier in the study area. Several studies from southern Alaska have found that ELA lowering was less than expected compared to the presumed temperature lowering during the LIA (Levy et al. 2004; Kathan 2006; Daigle

and Kaufman [2008]). In other words, assuming that the ELA is directly related to summer temperature, and that elevation changes in temperatures are determined by the lapse rate, then a typical 1°C cooling should correspond to a lowering of ELA of about 150 m. To evaluate whether ELA was lowered significantly less than expected during the LIA in the study area, a realistic estimate of the *maximum* ΔELA was calculated for each glacier. Only glaciers with well-defined moraines formed during the LIA were selected for ELA reconstruction.

The ELAs of the "modern" glaciers were determined using three-dimensional models of the glacier surfaces created in ArcGIS v 9.1. The models were created using glacier extents derived from 1:63,360-scale aerial photographs taken in 1978, and a 30 m USGS digital elevation model (DEM) of the region based on the same photographs. Because the glaciers in the study area retreated throughout the second half of the 20th century (indicated by USGS topographic maps, aerial photographs, and field-mapped extents), the 1978 glaciers were most likely not in equilibrium with climate, and the AAR is expected to be lower than for the equilibrium state. To estimate AAR for the "modern" glaciers, we examined mass-balance data for the two glaciers in southern Alaska with long-term records, Gulkana and Wolverine Glaciers (Fig. 1). The mass-balance data indicate an average AAR of 0.58 (Gulkana Glacier = 0.56, Wolverine Glacier = 0.59) from 1966 to 1978 (Dyurgerov et al. [2002]). Although these records are from glaciers located ~200 km from the study area, they show regional synchronicity and consistency in AAR, and probably serve as a fair estimate of AAR for the glaciers in this study because they bracket the study area both geographically and climatically. Therefore, a conservative, but realistic, AAR estimate of 0.55 was chosen for the "modern" glaciers, resulting in a more conservative maximum ΔELA estimate.

The maximum LIA extent was determined by photo-interpretative mapping of glaciogeomorphic evidence, and field checked at five sites within the headwater tributaries of Greyling and Hallet Lakes. The large LIA terminal moraines attest to the relative stability of these former glaciers. These extents were combined with the 1978 USGS DEM to model the LIA glacier surfaces. Consequently, the LIA glacier surface models underestimate the height of the LIA glacier surfaces; however, this is appropriate for maximum ΔELA estimates, because underestimating the height of the glacier surface in AAR reconstructions results in underestimating the LIA ELAs and a more conservative maximum ΔELA estimate. Following the same logic, an AAR of 0.65 was chosen for the reconstructed LIA glaciers, because this value is generally the maximum for stable alpine glaciers (Dyurgerov et al. [2002]).

Lake sediments

Core recovery

The bathymetries of both Hallet and Greyling Lakes were mapped prior to coring using a GPS-integrated sonar depth recorder. Sediment cores were recovered using a percussion corer operated from a floating platform, and shorter surface cores were taken with a gravity corer. Three percussion cores were collected from each lake. More information about the suite of cores is presented by McKay ([2007]). In this study, we focus on the longest and best-dated cores from the lakes. Percussion core HT01 was recovered from near the center of the lake with a water depth of 40.5 m, along with its companion surface core HT01B. Percussion core GY05 and surface core GY05A were recovered from the central sub-basin of Greyling Lake, which is semi-isolated from the primary inflows (Fig. 2).

Geochronology

A total of 20 radiocarbon (^{14}C) ages were analyzed from cores HT01 (11) and GY05 (9). Sediment samples between 0.5 and 2.0 cm thick were wet-sieved to isolate macrofossils. Eight samples were composed of woody and other terrestrial plant fragments. The other 12 samples comprised a mixture of terrestrial and aquatic plant material and chitin, which was concentrated within the 120–250 μm size fraction. The ^{14}C ages were calibrated and the median probability age was calculated using CALIB v 5.02 (Stuiver and Reimer [1993]). The top 10 cm of surface core HT01-B were analyzed using a combination of $^{239+240}$Pu and ^{137}Cs activities, and a constant-rate-of-supply (CRS) model using excess ^{210}Pb activities (Appleby and Oldfield [1978]). The $^{239+240}$Pu activity, obtained at 0.5 cm resolution to 10 cm depth, was measured using inductively coupled plasma mass

spectrometry. [210]Pb measurements were obtained at 0.5 cm resolution to 7 cm depth and measured by gamma spectrometry (Appleby 2001). Major-element geochemistry and shared morphology imaged with a scanning electron microscope were used to correlate a tephra at 180 cm depth in core HT01 with a tephra at 67 cm in core GY05 (McKay 2007). A ^{14}C age from 178.5 cm depth in core HT01 was then used to infer the age of the correlative tephra in core GY05. Smoothed cubic-spline functions were used to model the age-depth relations and the associated 95% confidence intervals (Heegaard et al. 2005). Maximum k-values ($k = n - 1$) were used for both age models to maximize the flexibility of the splines without over-interpreting changes in sedimentation rate. All ages are presented in calendar years prior to 1950 AD (cal BP).

Sedimentological and biological analyses

Magnetic susceptibility was measured at 0.5 cm intervals on the split core faces using a Bartington MS2 surface meter. Grain-size distributions were measured using a Coulter LS 230 laser diffraction particle-size analyzer. A total of 83 samples were taken from cores HT01 and GY05, and pretreated before analysis: The 0.2–0.4 g samples were heated overnight at 50°C with 10 ml of 30% H_2O_2 to remove organics, and heated for 4 h at 80°C with 10 ml of NaOH to dissolve biogenic silica. The pretreated samples were deflocculated by adding 10–15 ml of hexametaphosphate and shaking for 0.5 h before analysis. The mass-percent of the >1 mm size fraction was determined for 42, 5-cm-thick sections of core HT01 using a 1 mm sieve.

Percent organic matter (OM) and dry bulk density (DBD) were measured on 1 cm^3 samples taken at 2.5 cm intervals from cores HT01 and GY05. The top 10 cm of surface core HT01B was sampled at 0.5 cm intervals to develop a higher-resolution record for comparison to instrumental climate records. Samples were dried overnight at 70°C, allowed to cool to room temperature, and weighed to determine bulk density. The samples were then heated to 550°C for 5 h, cooled to room temperature in a desiccating chamber, and weighed to determine loss-on-ignition, which was used to approximate mass-percent OM.

Biogenic silica (BSi) was measured at 1 cm intervals over the top 2 m of core HT01, and at 5 cm intervals over the bottom 2.5 m of the core. Each sample was 0.5 cm thick, and taken from the core axis. The top 9 cm of surface cores HT01B and GY02A were sampled at 0.25 cm intervals to develop a high-resolution record for comparison to instrumental climate records. Samples were dried and ground to powder; large samples ($\sim$200 mg) were used for analysis because of the low BSi content in the sediment, and to reduce the effects of sample heterogeneity. The samples were pretreated to remove organic material (shaken overnight with 5 ml of 30% H_2O_2) and carbonate (shaken for 1 h with 5 ml of 1 M HCl). BSi was extracted with 40 ml of 10% Na_2CO_3 (4 h at 85°C), and concentrations were determined using molybdate-blue reduction and spectrophotometry, following Mortlock and Froelich (1989). A large reference sample taken from core HT01 was homogenized and run twice with each batch; the results were used to account for minor batch effects.

Glacial history

Hallet Lake valley

Lichen diameters were measured at 13 sites (Fig. 3a) in the forefields of glaciers that discharge to Hallet Lake. Maximum lichen thalli sizes for individual landforms ranged from 15 to 68 mm, corresponding to ages ranging from 1920 ± 20 to 980 ± 200 AD (Table 1). With the exception of station 13 located high on the largest lateral moraine of glacier HTG1 (Fig. 3a; Table 1), the lichenometric ages indicate that all of the prominent, bouldery moraines in the southern end of the valley stabilized after $\sim$1500 AD. Moraines deposited by glaciers on the west side of the valley record a restricted LIA advance (Fig. 3a), and lichen ages (1870–1920 AD) indicate that the moraines stabilized more recently. Also, in contrast to the moraine sequence in the southern part of the valley, older moraines are preserved beyond the maximum LIA extent in these cirques (Fig. 3a). These moraines are degraded, with lower crests and smaller, weathered, and more rounded boulders than the LIA moraines in the valley, but appear significantly younger than the rounded, vegetated moraines at the mouth of Hallet Valley, which are attributed to Wisconsinan advances in the region. Despite the presence of large lichens on the landforms (120–150 mm), an accurate age could not be obtained because of the non-circular growth

Table 1 Summary of lichen sizes on moraines in Hallet and Greyling Lake valleys

Lichen station (Fig. 3)	Latitude (°N)	Longitude (°W)	Maximum thallus diameter (mm)	Age (year before 2006)[a]	Age (year AD)[a]
Hallet Lake valley					
1	61.48031	146.23224	42	340	1670
2	61.48063	146.23138	38	280	1730
3	61.47974	146.28105	24	140	1870
4	61.48000	146.24053	31	200	1810
5	61.47714	146.22375	47	440	1570
6	61.47687	146.22279	43	360	1650
7	61.48023	146.21613	32	210	1800
8[b]	61.48097	146.21360	51	520	1490
9	61.48182	146.21289	43	360	1650
10	61.48207	146.21211	20	110	1900
11[b]	61.48505	146.20679	68	1030	980
12	61.48679	146.24397	15	90	1920
13	61.48947	146.24955	24	140	1870
Greyling Lake valley					
1	61.37254	145.74860	25	140	1870
2	61.37335	145.74854	46	420	1590
3	61.37055	145.74991	8	60	1950
4	61.36983	145.74675	33	220	1790
5	61.37018	145.74470	18	100	1910
6	61.36873	145.74618	40	310	1700
7	61.36848	145.74363	32	210	1800
8	61.37058	145.74206	32	210	1800
9	61.37052	145.74143	17	100	1910
10	61.37049	145.74030	44	380	1630
11	61.36838	145.73821	17	100	1910
12	61.36902	145.74020	34	230	1780
13	61.37104	145.73427	38	280	1730

[a] Based on the lichen growth curve for the Wrangell–St. Elias Mountains revised by Solimina and Calkin (2003)

[b] Ages calculated using the linear growth curve of Solomina and Calkin (2003)

patterns of the lichens, and the decreased certainty of ages for lichen thalli larger than 100 mm, calculated using the available growth curve for the Wrangell–St. Elias Mountains (Solomina and Calkin 2003). The single control point for lichens larger than 100 mm in this growth curve is the 130-mm-diameter lichen on a surface dated by ^{14}C to 2870 cal BP (Denton and Karlén 1973; Solomina and Calkin 2003). This age is therefore adopted as a best estimate for these landforms. Moraines with similar lichen sizes and weathering features were mapped in all four cirques in the western part of the watershed (Fig. 3a). In cirques 6 and 7, they occur beyond the maximum LIA moraines, and in cirque 8 they form the moraines

closest to the cirque headwall. This cirque lacks both modern glaciers and glacial deposits indicative of a LIA advance (Fig. 3a).

Greyling Lake valley

Lichens were measured on 13 landforms in the Greyling Lake valley (Fig. 3b). The maximum diameter of lichen thalli on individual landforms ranged from 8 to 46 mm, corresponding to ages ranging from 1950 ± 10 to 1590 ± 80 AD (Table 1). The lichen ages suggest that all of the bouldery moraines near Upper Greyling Lake are associated with LIA glacier advances. The LIA moraine sequence records a

complex history of advance and retreat from the multiple cirques: the west tongue of glacier GYG1 experienced limited advance compared with the other glaciers in the valley, but was the only glacier to preserve a record of several moraines deposited progressively down-valley during the LIA (Fig. 3b). Lichenometric ages suggest the glacier underwent several episodes of advances and standstills from 1630 to 1800 AD, when it reached its full extent, coalescing with the glacier emanating from the east near Upper Greyling Lake. The moraine record indicates that the east tongue of glacier GYG1, and the other glaciers in the valley (which are larger than the west tongue of GYG1) reached their LIA maximum extents earlier, between 1590 and 1730 AD (Fig. 3b). Recessional moraines record the pauses during the retreat of these larger glaciers, and suggest that most of the recession from the LIA maximum extents occurred during the past 100 years.

Equilibrium-line altitudes

ELAs for the study areas ranged from 1410 to 1650 m for the "modern" glaciers, and 1280 to 1610 m for the reconstructed maximum LIA glaciers. The calculated ELAs for both the "modern" and LIA reconstructions tend to rise to the west (3 m km^{-1}, $p = 0.009$). The average maximum ELA lowering (ΔELA) was 86 ± 61 m ($n = 7$) near Hallet Lake, and 82 ± 38 m ($n = 14$) near Greyling Lake. Because the ΔELA values are essentially equal, all 21 glaciers are used to estimate the maximum ΔELA for the area (83 ± 44 m, $n = 21$). The number of LIA glaciers is fewer than for "modern" glaciers because some of the glaciers coalesced during the LIA.

Lake sediments[1]

Geochronology

Hallet and Greyling Lakes age-depth models

Downcore changes in $^{239+240}$Pu and ^{137}Cs activities in the surface core from Hallet Lake (HT01-B) are

---

[1] Downcore data presented in this study are available on-line at the World Data Center for Paleoclimatology (ftp://ftp.ncdc. noaa.gov/pub/data/paleo/paleolimnology/northamerica/usa/alaska/ chugach2008.txt).
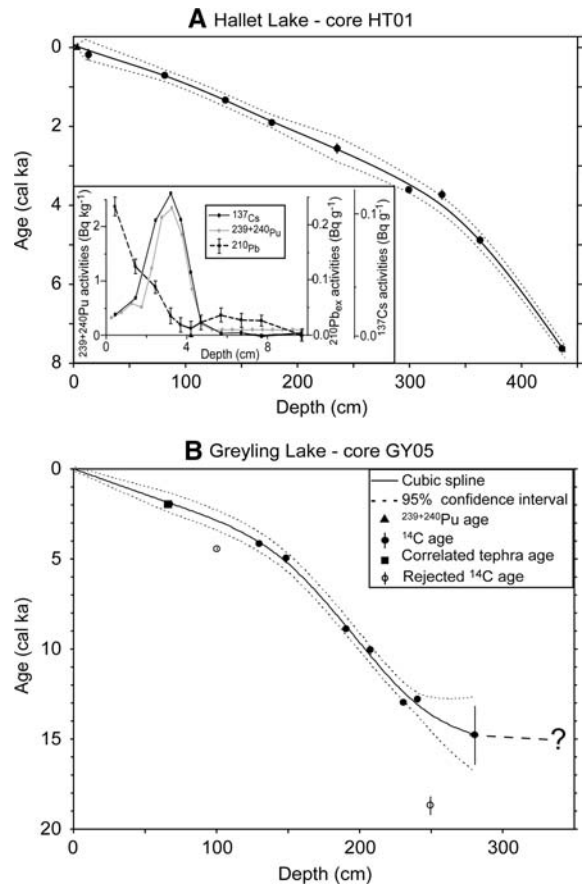

Fig. 4 Age-depth models for cores analyzed in this study, including (**a**) HT01 from Hallet Lake, and (**b**) GY05 from Greyling Lake. Inset in (**a**) shows the activity profiles of $^{239+240}$Pu, ^{210}Pb, and ^{137}Cs (data listed in McKay 2007). The tephra age in GY05 is based on correlation with a dated tephra in HT01. Depths have been adjusted to account for loss of sediment at the top of the core and, in core GY05, instantaneous sedimentation from 240 to 250 cm and 320 to 330 cm. The cubic spline and 95% confidence intervals were developed following the procedure of Heegaard et al. (2005) using maximum k values for flexible curves. Ages below 250 cm in core GY05 are not well known; we estimate the basal age at 15 ka. Error bars are 2σ ranges for the calibrated ^{14}C ages, and are smaller than the plot symbol in most cases (data listed in Table 2)

concordant and show a well-defined peak at 3.25 cm (Fig. 4b, inset; details in McKay 2007). We correlate this peak with the peak discharge from atmospheric atomic bomb testing in 1963 AD (Ketterer et al. 2004). The ^{210}Pb activity in core HT01-B is low, with relatively high analytical errors and a reversal from 3 to 6 cm (Fig. 4a). The low activity is typical of sediment in glacier-fed lakes, especially at high

latitudes, where low ^{210}Pb flux imposes a significant limitation (Wolfe et al. 2004). Despite this, the constant-rate-of-supply (CRS) model indicates an average sedimentation rate of 0.082 cm yr^{-1}, which is similar to the rate inferred from the $^{239+240}$Pu and ^{137}Cs peaks (0.076 cm yr^{-1}). To account for the reversal in ^{210}Pb activity, the model invokes a 15-year period of high sedimentation rate (~ 4 times higher than the rest of the 20th century) that is not supported by any sedimentological or climatological evidence. Also, the concentrations of BSi and OM do not decrease during this interval, as would be expected with a major change in clastic sedimentation rate. Because of this, and in light of the low

activities and relatively large errors, we are hesitant to adopt ages directly from the CRS model. Instead, we use the average sedimentation rate inferred from the $^{239+240}$Pu and ^{137}Cs peaks to determine ages for the top 10 cm of the core, and use the average rate derived from the ^{210}Pb CRS model as supporting evidence (see McKay (2007) for further discussion on the age of recent sediment).

An age-depth model for core HT01 was developed using all eleven calibrated ^{14}C ages (Table 2), one $^{239+240}$Pu age (3.25 cm = 1963), and the surface age (0 cm = 2006) obtained from the companion surface core (HT01B) (Fig. 4a). Two organic samples were analyzed in duplicate to assess any potential offset in

Table 2 Radiocarbon ages and complementary data

Lab ID[a]	Top depth (cm)[b]	Bottom depth (cm)[b]	Material type[c]	^{14}C age (BP)	±	Cal age (BP)[d] (median probability)	2σ range ±
Core HT01							
29497	10	11	TPF	190	15	175	140
29498	10	11	APF, TPF	120	15	110	130
29499	81.5	82	TPF	810	20	715	40
33138	135	137	<120 μm	1465	25	1350	40
29500	177	178	TPF	1975	15	1920	50
31584	177	178	<120 μm	1990	20	1940	50
29501	236	236.5	WS	2480	15	2585	120
33139	299	301	<120 μm	3395	25	3645	60
33140	329	331	<120 μm	3485	45	3760	110
31585	363	365	<120 μm	4360	30	4920	90
33141	435	440	WS	6875	15	7695	40
Core GY05							
33142	100	102	<120 μm	3975	30	5010	150
31587	130	130	WS	3800	15	4465	70
31588	149	149	WS	4435	15	4190	150
33143	190	192	<120 μm	8115	20	9030	60
41390	207	209	<120 μm	9080	60	10,240	160
33144	230	232	<120 μm	11,350	35	13,225	80
134208[e]	240	242	<120 μm	11,140	100	13,046	160
33145	260	262	<120 μm	15,840	310	19,085	500
33146	282	284	<120 μm	12,830	630	15,085	1660

[a] Analyses performed at the Keck Carbon Cycle AMS Facility at UC Irvine

[b] Depths adjusted for loss of 1 cm from the surface sediment and zones of instantaneous sedimentation from 240 to 250 cm and 320 to 330 cm

[c] TPF, terrestrial plant fragments; APF, aquatic plant fragments; WS, woody stems; <120 μm, chitin and detrital terrestrial and aquatic plant fragments between 250 and 120 μm

[d] The ^{14}C ages were calibrated using CALIB v 5.02 (Stuiver and Reimer 1993)

[e] The Center for Accelerator Mass Spectrometry at the Lawrence Livermore National Laboratory

the ^{14}C ages of terrestrial plant material compared with the mixture of aquatic and terrestrial. The resulting ages overlap within 1σ in both cases. A distinctive 0.5-cm-thick, clay-rich layer was used as a marker to tie together core HT01 and the associated surface core HT01-B. The correlation indicates that 2.3 cm of sediment was lost from the top of core HT01, and depths in the age model were adjusted accordingly. On the basis of this age model, the sedimentation rate from 7.8 to 4 ka averaged $\sim$0.03 cm yr^{-1} before increasing to $\sim$0.09 cm yr^{-1} from 4 ka through the present. The age at the base of the core (7.8 ka) probably approximates the timing of the emplacement of the debris avalanches that dam the lake.

Nine ^{14}C ages and the correlated tephra age (1926 $\pm$ 24 cal BP based on the pooled mean of the duplicate ages from 177 cm depth, 2 cm above the tephra) were used to develop the age model for core GY05 (Fig. 4b; Table 2). A series of clay-rich layers correlated from core GY05 across to surface core GY05A indicate that 1 cm of sediment was lost from the top of core GY05. Two ^{14}C ages were not included in the age model: the age from 100 cm was rejected because it fell off the well-defined nearly linear trend set by the four ages nearest to it in the core. The age from 250 cm was rejected because it suggested that the bottom was deposited >19 ka, which is unlikely considering previous studies have shown that the Chugach Range was occupied by extensive ice at that time (Hamilton and Thorson 1983). The age model is not well constrained over the lower 1 m of the core where sediment probably accumulated rapidly in an ice-proximal glaciolacustrine setting. On the basis of visual extrapolation, we assign an age of about 15 ka to the base of the core, which is consistent with the deglacial age near Matanuska Glacier, 130 km northwest of Greyling Lake (Yu et al. 2008). Like Hallet Lake, the sedimentation rate at Greyling Lake was low ($\sim$0.01 cm yr^{-1}) following deglaciation to 4 ka, increasing to $\sim$0.03 cm yr^{-1} from 4 ka to the present.

Sedimentological and biological analyses

Hallet Lake

Core HT01 is dominated by silty mud, and is weakly laminated to bedded throughout the core (0.1–2-cm-thick laminations) (Fig. 5a). The laminations are defined by changes in color, and in places by slight changes in texture. The sedimentary sequence includes three main units: (Unit I) The bottom of the core, from 450 to 340 cm (7.8–4.3 ka), consists of dark-gray (10YR 2/1) silty mud, with abundant angular rock fragments. (Unit II) Laminated, dark-gray (10YR 2/1) mud with few rock fragments is present from 340 to 160 cm (4.3–1.6 ka). (Unit III) Above 160 cm, the laminations thin, and the sediment color varies from light gray (10YR 3/1) to light tan (10YR 4/6). Magnetic susceptibility (MS) is low ($\sim$30 $\times$ 10^{-6} SI), with minimal variability punctuated by a large peak ($\sim$250 $\times$ 10^{-6} SI) corresponding to the single tephra layer at 180 cm (1926 cal BP = 24 AD). The sediment matrix is fine grained (median grain size typically <4 μm) with no significant downcore trends. The mass percent of particles >1 mm is highest below 340 cm, consistent with the visible lithostratigraphy. OM is generally low, varying from 2.5% to 7.3%. OM is highest near the base of the core and is inversely related to bulk density. BSi ranges from 4 to 100 mg BSi g^{-1} dry sediment. BSi is very high at the base of the core (25–100 mg g^{-1}). It decreases at 390 cm depth (5.5 ka), then again at 350 cm (4.5 ka). BSi remains low with minor variability (4–20 mg g^{-1}) above 350 cm. DBD ranges from 0.7 to 1.5 g cm^{-3}, generally increasing towards the top of the core, with pronounced low-frequency variability.

Greyling Lake

Core GY05 consists of three main stratigraphic units (Fig. 5b): Unit I, the basal unit from 350 to 230 cm (15 (?)–12.5 ka) is composed of gray (5GY 3/1) silty mud, which is generally not laminated, although a zone with well-defined laminae (0.5–1-cm-thick) is located from 350 to 330 cm. Two large rock clasts (7 and 10 cm long by 7 cm wide) were recovered in this unit, from about 250 to 330 cm. Unit II from 230 to 130 cm (12.5–4 ka) is grayish-green (5GY 6/3) organic-rich silty clay, with a sharp contact at the base, and a gradational contact at the top. Unit III from 130 to 0 cm (4–0 ka) is thinly bedded, gray to dark-gray clayey mud. MS is generally low throughout the core ($\sim$20 $\times$ 10^{-6} SI); its first-order trend is consistent with the core lithology, with the lowest values ($\sim$5 $\times$ 10^{-6} SI) in organic-rich unit II. Downcore changes in grain size can be subdivided into three zones, consistent with the lithostratigraphic

Fig. 5 Lithostratigraphy, magnetic susceptibility, dry bulk density, organic-matter content, and median grain size for cores (**a**) HT01 and (**b**) GY05 from Hallet and Greyling Lakes, respectively. Biogenic-silica content and particles >1 mm for core HT01 from Hallet Lake are also shown in (**a**). Smoothed line for bulk density and organic matter are 5-point running means. All data listed in McKay (2007). Age scale based on models shown in Fig. 4
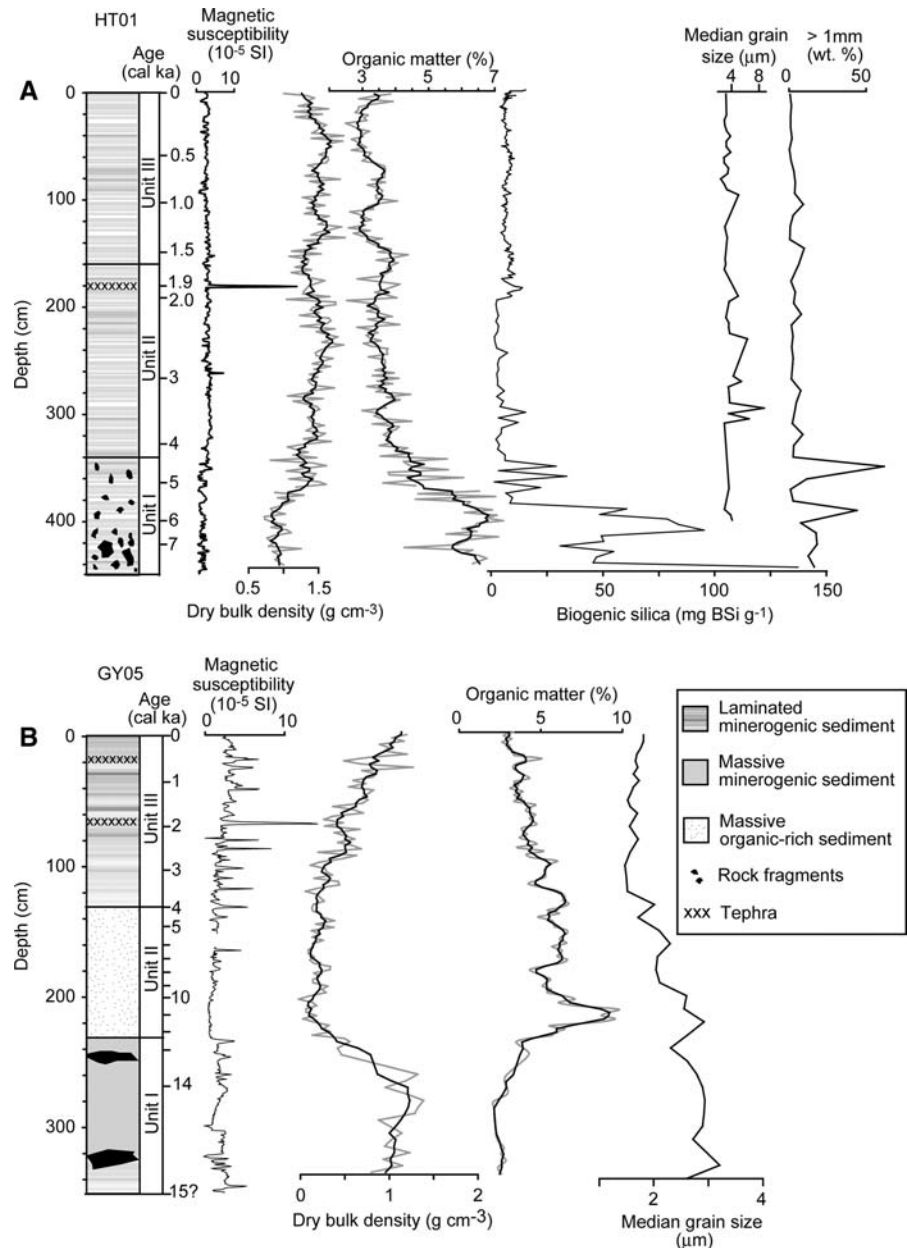
units; generally the sediment matrix fines towards the surface, except during the last 4 ka when it coarsened slightly. OM ranges from 2.1% to 9.7%, is highest in unit II, and lower in units I and III. DBD ranges from 0.5 to 1.5 g cm^{-3}, and shows the opposite trend as OM. BSi was analyzed in the top 10 cm of the surface sediment, and at several depths deeper in core GY05, but was generally undetectable relative to background concentration.

Sediment bulk density, organic-matter content, and glacier variability

The strong similarity between century-scale variations in the OM of sediment at Hallet and Greyling Lakes (Fig. 6) suggests that the glacier-lake systems respond to regional climate variability on multiple timescales. OM, determined by loss-on-ignition (LOI), has been widely used to infer glacier variability, and
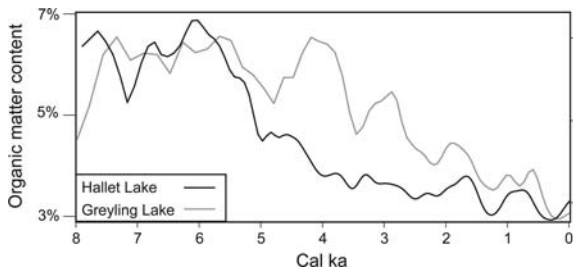
Fig. 6 Organic matter content (OM) in sediment cores from Hallet and Greyling Lakes over the past 8 ka. The data have been smoothed using a Gaussian-weighted low pass filter. Ages are based on models shown in Fig. 4

environmental and climatic change, especially at high-latitude and glacier-fed lakes (e.g., Willemse and Törnquist 1999; Kaplan et al. 2002; Nesje et al. 2004). OM is primarily controlled by the flux of organic material deposited, the clastic sedimentation rate and DBD. In proglacial lakes, the clastic sedimentation rate is primarily controlled by the activity of the glaciers, and is often more variable than the contribution of organic material, thereby driving the OM concentrations (Nesje et al. 2004).

On multi-decadal timescales, DBD of sediment deposited in proglacial lakes is often controlled by the amount of glacially derived sediment, which is related to the size and activity of glaciers in the headwaters (e.g., Leonard 1985; Noon et al. 2000; Bakke et al. 2005). Because sediment younger than about 4 ka from both Hallet and Greyling Lakes is dominantly glacial and minerogenic (94–98%), the fluctuations in DBD (0.5–1.5 g cm^{-3}) on centennial and longer timescales are most likely attributable to changes in glacier activity. Once again, because the concentration of organic matter and the DBD of the sediments are inversely related to glacier activity, their quotient (OM) is probably most sensitive to glacier size.

OM and DBD are both indicative of glacier activity, but they are not independent variables. They are related mathematically: DBD is directly proportional to the mass of dry sediment, which is used to calculate LOI. They are also related physically: increased OM reduces DBD because the density of organic material is low, and because it provides flocculation nuclei and affects sediment packing. Finally, at Hallet and Greyling Lakes, OM and DBD are related mechanistically, because both DBD and OM are driven, in part, by glacier activity in the headwaters. These interrelations are evident in the

similarities between OM and DBD at both lakes (Fig. 5). Despite their overall similarities, the records contain notable differences, reinforcing the importance of a multiproxy approach.

Holocene climate variability and glacial history at Hallet and Greyling Lakes

Early Holocene warmth

From 10 to 6 ka, sediment deposited in Hallet and Greyling Lakes was characterized by low accumulation rates, elevated OM, and low DBD (Fig. 5). These characteristics are consistent with general warmth, increased productivity, and diminished, if not entirely ablated, glaciers in the lake valleys. This is generally consistent with evidence of 2–3°C warming in Alaska during the early Holocene (Kaufman et al. 2004). BSi in Hallet Lake is nearly an order of magnitude higher (60–100 mg g^{-1}) from the base of the core (7.8 ka) to 5.6 ka than for the rest of the sediment sequence (4–20 mg g^{-1}). Although some of this difference is attributable to lower sedimentation rates and bulk density (average BSi flux is only 2–3 times higher), the dramatic shift highlights the non-linear BSi-climate relation discussed by McKay et al. (2008).

Neoglaciation

The onset of Neoglaciation in the region is clearly recorded in the sediment sequences. At Greyling Lake, OM began to decrease, and DBD began to increase ca. 4 ka (Fig. 5b), consistent with a three-fold increase in the sedimentation rate at the same time (Fig. 4). This shift is also manifest in the lithostratigraphy of core GY05 as the gradational contact from the massive organic-rich sediment of Unit II to the laminated minerogenic sediment of Unit III at 130 cm (Fig. 5b). From 4 ka to present, OM (DBD) in Greyling Lake generally decreases (increases), with the lowest (highest) values during the LIA. This is consistent with the glacial geomorphology, which indicates that no Holocene moraines older than the LIA were preserved in Greyling Lake valley.

At Hallet Lake, OM begins to decrease ca. 4.5 ka, at which time the BSi values reach a stable low value that is generally maintained through the present. Like Greyling Lake, the age model for Hallet Lake

indicates a three-fold increase in sedimentation rate after 4 ka (Fig. 4a). However, the DBD begins to increase much earlier, rapidly rising from 5.5 to 4.0 ka to a maximum at ~2.5 ka and remaining generally high to the present. We suggest that the onset of Neoglaciation in both of the lake valleys occurred between 4.5 and 4.0 ka, and is manifested in OM and sedimentation-rate changes in both sediment records. The onset of Neoglaciation at Hallet and Greyling Lakes appears to have begun somewhat earlier than elsewhere in southern Alaska; there is evidence of Neoglacial advances in the Kenai Mountains beginning at 3.6 ka (Wiles and Calkin 1994), advances in the Ahklun Mountains at 3.1 ka (Levy et al. 2004), and dramatic cooling and increased storminess around the Gulf of Alaska ca. 3.5 ka (Calkin et al. 2001).

The early increase in DBD at Hallet Lake may be best described as a transitional period; however, the differences in the Hallet and Greyling Lake DBD records may be due to distinct patterns of glacier fluctuations in the valleys during Neoglaciation. The only Neoglacial moraines preserved beyond the maximum LIA extent in either valley are in the three cirques on the west side of the Hallet Lake valley (Fig. 3). The ages of these moraines are not well constrained, but are estimated based on lichen size at ca. 2.9 ka. The formation of these moraines may correlate with the DBD peak in Hallet Lake at 2.5 ka. The differences between the glaciolacustrine sequences at Hallet and Greyling Lakes might also be attributed to the presence of Upper Greyling Lake, which serves as a sediment trap in Greyling Lake valley. In contrast, Hallet Lake is directly connected to the discharge of glaciers in its catchment.

First millennium AD cooling and glacier advances

BSi-inferred summer temperatures at Hallet Lake from ~100 to 500 AD were 1°C warmer than the long-term (2 ka) average (3.1°C), before decreasing rapidly to ~2°C by 600 AD (Fig. 7) (McKay et al. 2008). Following this cooling, summer temperatures remained below the 2 ka average, slowly rising to ~3°C by 800 AD. This is broadly consistent with regional (e.g., Hu et al. 2001) and hemispheric (e.g., Moberg et al. 2005) proxy records. The cooling from ~480 to 600 AD also coincides with glacial

advance in southern Alaska. Glacier forefields in the Chugach Range, as well as the Kenai and St. Elias Mountains, show evidence of first millennium AD (FMA) advances (Wiles et al. 2008). Radiocarbon ages from glacially overrun trees suggest that the main interval of advance was between 590 and 650 AD; an age of 430 AD is the earliest evidence of glacial expansion for the coastal mountain ranges (Wiles et al. 2008). The DBD record from Hallet Lake is also consistent with FMA advances in the valley; DBD is low from ~1 to 400 AD before peaking at ~700 AD, and remains high until ~850 AD. OM is also consistent with glacial expansion at the time, decreasing markedly from 400 to 600 AD. No glaciogeomorphic evidence of FMA advances has been found in Hallet or Greyling Lake valleys, suggesting that the landforms were subsequently overrun by LIA advances.

Medieval Period

After ~600 AD, BSI-inferred summer temperature gradually increased from ~2 to 3°C through ~1100 AD, before rapidly increasing to ~4°C by 1300 AD, and remained above average until ~1500 AD (Fig. 7) (McKay et al. 2008). While the temperature reconstruction from Hallet Lake suggests warming throughout the period, summer temperature did not reach its maximum until 1300–1500 AD. The Medieval Warm Period (MWP) is classically considered to have occurred significantly earlier, from ~950 to 1200 AD (Brázdil et al. 2005); however, many studies have highlighted the spatial and temporal heterogeneity of the warm period (e.g., Hughes and Diaz 1994; Jones and Mann 2004; Osborn and Briffa 2006). The warming between 1300 and 1500 AD in Hallet Lake is consistent with a period of general warmth observed in proxy records throughout the Northern Hemisphere.

In southern Alaska, only a few studies have presented well-constrained evidence for the timing and magnitude of the MWP (Hu et al. 2001; Loso et al. 2006; Loso this volume; Wiles et al. 2008). Tree-ring chronologies from recently uncovered subfossil wood in glacial forefields in the Chugach and Kenai Mountains (Fig. 1) suggest continuous forest growth from ~900 to 1200 AD in areas that were covered with ice during the FMA and the LIA (Wiles et al. 2008). The quantitative temperature
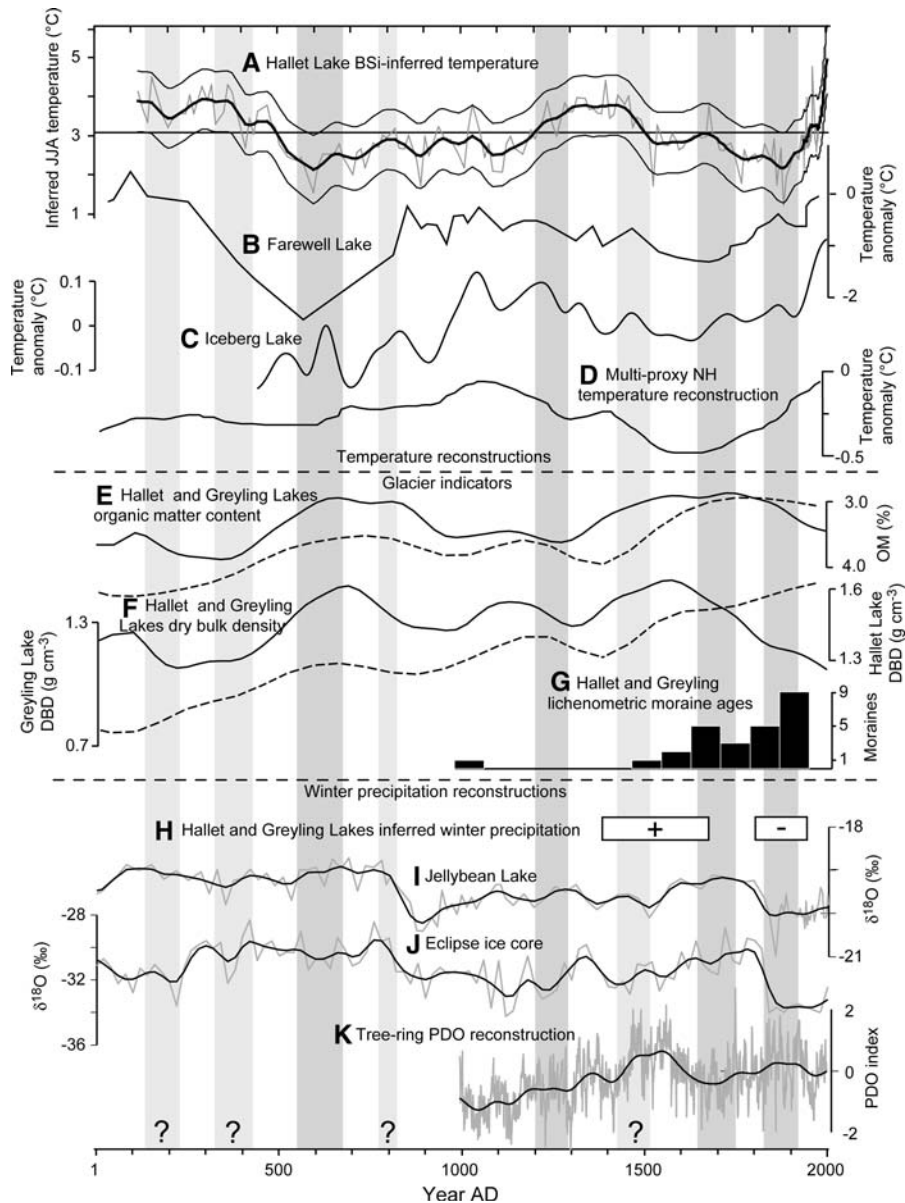
Fig. 7 Comparison of regional and hemispheric proxy temperature and precipitation records for the last 2 ka. (**a**) Summer (JJA) temperature based on biogenic-silica (BSi) content at Hallet Lake (McKay et al. 2008). Horizontal line indicates the mean of the last 2 ka. Thin curves are confidence intervals determined as the dynamic RMSEP$_{(boot)}$. (**b**) Isotope-inferred temperature from Farewell Lake, northwestern Alaska Range (Hu et al. 2001). (**c**) Varve-thickness-inferred summer temperature from Iceberg Lake, eastern Chugach Range (Loso this volume). (**d**) Multi-proxy Northern Hemisphere temperature reconstruction (Moberg et al. 2005). (**e**) Organic matter content (OM) of sediment from Hallet (solid line) and Greyling (dashed line) Lakes (this study). (**f**) Dry bulk density (DBD) of sediment from Hallet Lake (solid line) and Greyling Lake (dashed line) (this study). (**g**) Lichenometric age ranges for moraines in Hallet and Greyling Lake valleys (this study). (**h**) Periods of increased (+) and decreased (−) winter precipitation, inferred from the combination of summer temperature at Hallet Lake and evidence for glacier expansion at Hallet and Greyling Lakes (this study). See text for details. (**i**) Oxygen isotope ($\delta^{18}O$) variations in CaCO$_3$ from Jellybean Lake sediments (Anderson et al. 2005). (**j**) $\delta^{18}O$ variations in the Eclipse ice core from Mount Logan (Fisher et al. 2004). (**k**) Tree-ring-inferred Pacific Decadal Oscillation index (PDO) (MacDonald and Case 2005). Dark shaded intervals are well-constrained periods of expanded mountain glaciers in southern Alaska, poorly constrained periods are lightly shaded and denoted with a question mark (Wiles et al. 2008). For all records, gray curves are raw time series, and black curves are low-pass filtered series. Site locations shown in Fig. 1

reconstruction from Farewell Lake, in the foothills of the northwestern Alaska Range (Fig. 1) (Hu et al. 2001), indicates a period of increased temperature (∼0.5°C cooler than modern) from ∼800 to 1500 AD. The 1600 year varve sequence from Iceberg Lake in the eastern Chugach Mountains (Fig. 1) contains a period of increased varve thickness from 1000 to 1300 AD (Loso et al. 2006; Loso this volume). Tree-ring series from coastal Alaska suggest general warmth from 900 to 1100 AD, as well as shorter periods of warm temperature centered on 1300 and 1450 AD (Barclay et al. 2003; D'Arrigo et al. 2006). The period of warmth inferred from the Hallet Lake BSi record from 1300 to 1500 AD is generally consistent with other records in the region, but the cooler summer temperature between 900 and 1200 AD is not consistent with other records of warm-season temperature from the area. Fluctuations in DBD and OM at Hallet Lake suggest that glaciers retracted from ∼850 to 1050 AD, consistent with evidence of glacial recession in the coastal ranges (Wiles et al. 2008).

Little Ice Age

The LIA in southern Alaska has been divided into three phases (early, middle, and late) based on glacial evidence and tree-ring chronologies (Wiles et al. 1999; Barclay et al. 2003). An increase in DBD and a decrease in OM in both Hallet and Greyling Lakes around ∼1050–1200 AD (Fig. 7) suggest that the glaciers in the lake valleys expanded during the early phase of the LIA. This is consistent with evidence of glacier expansion from 1180 to 1300 AD at several glaciers in the coastal ranges (Wiles et al. 2008). No terminal moraines from this advance are preserved in Hallet or Greyling Lake valleys, which is typical for this advance in southern Alaska (Wiles et al. 2008); however, a lichenometric age of 980 ± 200 AD from high on a lateral moraine in Hallet Lake valley (Fig. 3a) may be associated with this advance. DBD was low, and OM was high, from ∼1250 to 1350 AD, suggesting that the glaciers retreated as summer temperatures increased during the interval (Fig. 7) (McKay et al. 2008).

At both lakes, DBD increased from ∼1350 to 1400 AD, and remained high until 1750 AD. At Greyling Lake, DBD remained high through the present. OM at the lakes decreased during the same

interval, reaching a minimum at Hallet Lake at ∼1700 AD, and at ∼1800 AD at Greyling Lake. This is consistent with the glacial geomorphic evidence, which indicates that the largest LIA terminal moraines in Hallet and Greyling Lake valleys stabilized between 1550 and 1800 AD. Summer temperatures at Hallet Lake remained near the 2 ka average until ∼1700 AD (Fig. 7) (McKay et al. 2008). This suggests that the glacier advance associated with the middle phase of the LIA, which was the largest Holocene advance for most of the glaciers in the study area, began while the summer temperatures were fairly warm. This suggests a significant increase in winter precipitation during the interval. Evidence for increased winter precipitation in the region is supported by the peak in oxygen-isotope ratios in diatoms from Mica Lake during this interval (Schiff et al. this volume). A tree-ring-based reconstruction of the Pacific Decadal Oscillation (PDO) indicates that North Pacific sea surface temperatures were generally warm from 1350 to 1550 AD, which is also consistent with a deepened Aleutian Low and enhanced winter precipitation in southern Alaska (Fig. 7) (MacDonald and Case 2005). The winter-precipitation-sensitive isotopic records from the Eclipse ice core and Jellybean Lake sediments do not show this increase (Fisher et al. 2004).

By 1800 AD, BSi-inferred summer temperature was nearly 1°C below the 2 ka average. The 19th century was the coldest sustained interval in the BSi-inferred summer temperature reconstruction (McKay et al. 2008), and is consistent with several dendro-climate studies from southern Alaska (Barclay et al. 2003; Davi et al. 2003; Wilson et al. 2007). DBD in Hallet Lake decreased, and OM increased, from ∼1750 AD to the present, although part of this trend may be due to differential compaction near the top of the core; at Greyling Lake OM increased slightly, and DBD did not decrease during this interval. Recessional moraines dating to this interval suggest that the glaciers at the south ends of Hallet and Greyling Lake valleys stabilized during the late LIA, but glaciers were less extensive than during the middle LIA advances, despite the cooler summer temperatures, suggesting a reduction in winter precipitation.

The relatively limited lowering of ELA (ΔELA) during the maximum LIA is also consistent with the inference that snowfall was reduced. In this study, glacier geometry (the AAR method) was used to

estimate ELAs based on the mapped glacier extents. For "modern" glaciers, the calculated ELAs are therefore controlled by the integrated effects of climate over the few decades prior to 1978. At Hallet Lake, the period from 1950 to 1978 AD was on average 1.5°C warmer than during the maximum LIA cooling (McKay et al. 2008). Assuming that the ELA is strictly a function of summer temperature, and applying a regional environmental lapse rate of 7°C km^{-1} (McKay 2007), suggest that ELA should have lowered by ~210 m to account for the 1.5°C cooling. The *maximum* ELA lowering calculated using the maximum LIA glacier extents and the AAR method is, however, only 83 m. This ΔELA is a realistic maximum estimate, and is relatively insensitive to changes in AAR; to achieve the hypothetical lowering of ~210 m, the "modern" AAR would have to be ≤0.05. Evidence for reduced winter precipitation during the LIA has been identified in other glacial records from southern Alaska (Levy et al. 2004; Kathan 2006; Daigle and Kaufman 2008). Oxygen isotopes from the Eclipse ice core and Jellybean Lake sediments suggest a weakened Aleutian Low after 1800 AD (Fisher et al. 2004; Anderson et al. 2005). Oxygen isotopes in diatoms from Mica Lake also indicate that the Aleutian Low was generally weaker during the mid 19th century, then strengthened through the 20th century (Schiff et al. this volume).

Summary and conclusions

By integrating glaciogeomorphic and paleolimnological evidence from nearby, but hydrologically isolated drainage basins, we are able to infer multiple aspects of Holocene glacier and climate variability in the northeast Chugach Mountains:

(1) The early Holocene (from 10 to 6 ka) was generally warm, with diminished or entirely ablated glaciers in the cirques that presently contain glaciers in the headwaters of Hallet and Greyling Lakes.

(2) Moraine sequences and glaciolacustrine sediment indicate that the history of Neoglaciation was somewhat different in the Hallet and Greyling Lake valleys; however, nearly synchronous changes in OM and sedimentation rate in the two lakes suggest that Neoglaciation in the region began between 4.5 and 4.0 ka.

(3) Increased DBD and decreased OM of sediment in both lakes suggest that glaciers advanced during the first millennium AD, consistent with cooler summer temperatures inferred from BSi concentration at Hallet Lake (McKay et al. 2008). No glaciogeomorphic evidence of these advances was found, however, suggesting that the older moraines were subsequently overrun during the LIA.

(4) Lichenometric ages of large terminal moraines in both valleys and high DBD in Hallet and Greyling Lake sediments suggest that the LIA maximum advance occurred during the middle phase of the LIA, from 1550 to 1750 AD. The large glaciers, coupled with nearly average BSi-inferred summer temperatures during the interval suggest that increased winter precipitation drove the glacial expansion.

(5) The late phase of the LIA was the coldest of the past 2 ka, and is recorded by end moraines in most glacier forefields. Given the relatively limited glacier expansion and the cold summer temperatures, winter precipitation, driven by the strength of the Aleutian Low, was most likely reduced during this interval.

References

Anderson L, Abbott MB, Finney BP, Edwards ME (2005) Palaeohydrology of the southwest Yukon territory, Canada, based on multiproxy analyses of lake sediment cores from a depth transect. Holocene 15:1172–1183. doi:10.1191/0959683605hl889rp

Appleby PG (2001) Chronostratigraphic techniques in recent sediments. In: Last WS, Smol JP (eds) Tracking environmental change using lake sediments. Volume 1: Basin analysis, coring and chronological techniques. Kluwer Academic Publishers, Dordrecht, The Netherlands, pp 172–203

Appleby PG, Oldfield F (1978) The calculation of ^{210}Pb dates assuming a constant rate of supply of unsupported ^{210}Pb to the sediment. Catena 5:1–8. doi:10.1016/S0341-8162(78)80002-2

Bakke J, Lie Ø, Nesje A, Dahl SO, Paasche Ø (2005) Utilizing physical sediment variability in glacier-fed lakes for continuous glacier reconstructions during the Holocene, northern Folgefonna, western Norway. Holocene 15:161–176. doi:10.1191/0959683605hl797rp

Barclay DJ, Wiles GC, Calkin PE (2003) An 850 year record of climate and fluctuations of the iceberg-calving Nellie Juan Glacier, south central Alaska, U.S.A. Ann Glaciol 36:51–56. doi:10.3189/172756403781816419

Brázdil R, Pfister C, Wanner H, Storch HV, Luterbacher JR (2005) Historical climatology in Europe—the state of the art. Clim Change 70:363–430. doi:10.1007/s10584-005-5924-1

Calkin PE, Wiles GC, Barclay DJ (2001) Holocene coastal glaciation of Alaska. Quat Sci Rev 20:449–461. doi:10.1016/S0277-3791(00)00105-0

Daigle TA, Kaufman DS (2008) Holocene climate inferred from glacier extent, lake sediment and tree rings at Goat Lake, Kenai Mountains, Alaska, USA. J Quat Sci. doi:10.1002/jqs.1166

D'Arrigo R, Wilson R, Jacoby G (2006) On the long term context for late twentieth century warming. J Geophys Res 111:D03103. doi:10.1029/2005JD006352

Davi N, Jacoby G, Wiles G (2003) Boreal temperature variability inferred from maximum latewood density and tree-ring width data, Wrangell Mountain region, Alaska. Quat Res 60:252–262. doi:10.1016/j.yqres.2003.07.002

Denton GH, Karlén W (1973) Lichenometry: its application to Holocene moraine studies in Southern Alaska and Swedish Lapland. Arct Alp Res 5:347–372. doi:10.2307/1550128

Dyurgerov M, Meier M, Armstrong RL (2002) Glacier mass balance and regime: data of measurements and analysis. INSTAAR occasional paper no. 55. Institute of Arctic and Alpine Research, University of Colorado, Colorado

Fisher DA, Wake C, Kreutz K, Yalcin K, Steig E, Mayewski P, Anderson L, Zheng J, Rupper S, Zdanowicz C, Demuth M, Waszkiewicz M, Dahl-Jensen D, Goto-Azuma K, Bourgeois JB, Koerner RM, Sekerka J, Osterberg E, Abbott MB, Finney BP, Burns SJ (2004) Stable isotope records from Mount Logan, Eclipse ice cores and nearby Jellybean Lake. Water cycle of the North Pacific over 2000 years and over five vertical kilometres: sudden shifts and tropical connections. Géog Phys Quatern 58:337–352

Hamilton TD, Thorson RM (1983) The Cordilleran ice sheet in Alaska. In: Porter SC (ed) Late quaternary environments of the United States. Vol. 1, the Late Pleistocene. University of Minnesota Press, University of Minnesota, Minneapolis, pp 38–52

Heegaard E, Birks HJB, Telford RJ (2005) Relationships between calibrated ages and depth in stratigraphical sequences: an estimation procedure by mixed-effect regression. Holocene 15:612–618. doi:10.1191/0959683605hl836rr

Hu FS, Ito E, Brown TA, Curry BB, Engstrom DR (2001) Pronounced climatic variations in Alaska during the last two millennia. Proc Natl Acad Sci USA 8:1–5

Hughes MK, Diaz HF (1994) Was there a "Medieval Warm Period," and if so, where and when? Clim Change 26:109–142. doi:10.1007/BF01092410

Jones PD, Mann ME (2004) Climate over past millennia. Rev Geophys 42:1–42. doi:10.1029/2003RG000143

Kaplan MR, Wolfe AP, Miller GH (2002) Holocene environmental variability in southern Greenland inferred from lake sediments. Quat Res 58:149–159. doi:10.1006/qres.2002.2352

Kathan K (2006) Late Holocene climate fluctuations at Cascade Lake, northeastern Ahklun Mountains, southwestern Alaska. M.S. thesis, Northern Arizona University, Flagstaff, AZ, p 120

Kaufman DS, Ager TA, Anderson NJ, Anderson PM, Andrews JT, Bartlein PT, Brubaker LB, Coats LL, Cwynar LC, Duvall ML, Dyke AS, Edwards ME, Eisner WR, Gajewski K, Geirsdottir A, Hu FS, Jennings AE, Kaplan MR, Kerwin MW, Lozhkin AV, MacDonald GM, Miller GH, Mock CJ, Oswald WW, Otto-Bliesner BL, Porinchu DF, Ruhland K, Smol JP, Steig EJ, Wolfe BB (2004) Holocene thermal maximum in the western Arctic (0–180°W). Quat Sci Rev 23:529–560. doi:10.1016/j.quascirev.2003.09.007

Ketterer ME, Hafer KM, Jones VJ, Appleby PG (2004) Rapid dating of recent sediments in Loch Ness: inductively coupled plasma mass spectrometric measurements of global fallout plutonium. Sci Total Environ 322:221–229. doi:10.1016/j.scitotenv.2003.09.016

Leonard EM (1985) Glaciological and climatic controls on lake sedimentation, Canadian Rocky Mountains. Z Gletsch kd Glazialgeol 21:35–42

Levy LB, Kaufman DS, Werner A (2004) Holocene glacier fluctuations, Waskey Lake, northeastern Ahklun Mountains, southwestern Alaska. Holocene 14:185–193. doi:10.1191/0959683604hl675rp

Loso MG Summer temperatures during the Medieval Warm Period and Little Ice Age derived from varved proglacial lake sediments in southern Alaska. J Paleolimnol (this volume). doi: 10.1007/s10933-008-9264-9

Loso MG, Anderson RS, Anderson SP, Reimer PJ (2006) A 1500-year record of temperature and glacial response inferred from varved Iceberg Lake, southcentral Alaska. Quat Res 66:12–24. doi:10.1016/j.yqres.2005.11.007

MacDonald GM, Case RA (2005) Variations in the Pacific Decadal Oscillation over the past millennium. Geophys Res Lett 32:L08703. doi:10.1029/2005GL022478

McKay NP (2007) Late Holocene climate at Hallet and Greyling Lakes, central Chugach Range, south-central Alaska. M.S. thesis, Northern Arizona University, Flagstaff, AZ, p 96

McKay NP, Kaufman DS, Michelutti N (2008) Biogenic silica concentration as a high-resolution, quantitative temperature proxy at Hallet Lake, south-central Alaska. Geophys Res Lett 35:L05709. doi:10.1029/2007GL032876

Meier MF, Post AS (1962) Recent variations in mass net budgets of glaciers in western North America. IASH Publ 58:63–77

Moberg A, Sonechkin DM, Holmgren K, Datsenko NM, Karlen W, Lauritzen SE (2005) Highly variable Northern Hemisphere temperatures reconstructed from low- and high-resolution proxy data. Nature 433:613–617. doi:10.1038/nature03265

Mortlock RA, Froelich PN (1989) A simple method for the rapid determination of biogenic opal in pelagic marine sediments. Deep-Sea Res 36:1415–1426. doi:10.1016/0198-0149(89)90092-7

Nesje A, Dahl SO, Lie Ø (2004) Holocene millennial-scale summer temperature variability inferred from sediment parameters in a non-glacial mountain lake: Danntjørn, Jotunheimen, central southern Norway. Quat Sci Rev 23:2183–2205. doi:10.1016/j.quascirev.2004.08.015

Noon PE, Birks HJB, Jones VJ, Ellis-Evans JC (2000) Quantitative models for reconstructing catchment ice-extent using physical–chemical characteristics of lake sediments. J Paleolimnol 25:375–392. doi:10.1023/A:1011193401627

Osborn G, Menounos B, Koch J, Clague JJ, Vallis V (2007) Multi-proxy record of Holocene glacial history of the Spearhead and Fitzsimmons ranges, southern Coast Mountains, British Columbia. Quat Sci Rev 26:479–493. doi:10.1016/j.quascirev.2006.09.003

Osborn TJ, Briffa KR (2006) The spatial extent of 20th-century warmth in the context of the past 1200 years. Science 311:841–844. doi:10.1126/science.1120514

Papineau JM (2001) Wintertime temperature anomalies in Alaska correlated with ENSO and PDO. Int J Climatol 21:1577–1592. doi:10.1002/joc.686

Rodionov SN, Overland JE, Bond NA (2005) The Aleutian low and winter climatic conditions in the Bering Sea. Part I: Classification. J Clim 18:160–177. doi:10.1175/JCLI3253.1

Schiff CJ, Kaufman DS, Wolfe AP, Dodd J, Sharp Z Late Holocene storm-trajectory changes inferred from the oxygen isotope composition of lake diatoms, south Alaska. J Paleolimnol (this volume). doi: 10.1007/s10933-008-9261-z

Solomina O, Calkin PE (2003) Lichenometry as applied to moraines in Alaska, USA, and Kamchatka, Russia. Arct Antarct Alp Res 35:129–143. doi:10.1657/1523-0430(2003)035[0129:LAATMI]2.0.CO;2

Stuiver M, Reimer PJ (1993) Extended ^{14}C data base and revised CALIB 3.0 ^{14}C age calibration program. Radiocarbon 35:215–230

Wiles GC, Calkin PE (1994) Late Holocene, high-resolution glacial chronologies and climate, Kenai Mountains, Alaska. Geol Soc Am Bull 106:281–303. doi:10.1130/0016-7606(1994)106<0281:LHHRGC>2.3.CO;2

Wiles GC, Barclay DJ, Calkin PE (1999) Tree-ring-dated Little Ice Age histories of maritime glaciers from western Prince William Sound. Holocene 9:163–173. doi:10.1191/095968399671927145

Wiles GC, Barclay DJ, Calkin PE, Lowell TV (2008) Century to millennial-scale temperature variations for the last two thousand years indicated from glacial geologic records of southern Alaska. Glob Planet Change 60:115–125. doi:10.1016/j.gloplacha.2006.07.036

Willemse NW, Törnquist TE (1999) Holocene century-scale temperature variability from West Greenland lake records. Geology 27:580–584. doi:10.1130/0091-7613(1999)027<0580:HCSTVF>2.3.CO;2

Wilson R, Wiles G, D'Arrigo R, Zweck C (2007) Cycles and shifts: 1300 years of multi-decadal temperature variability in the Gulf of Alaska. Clim Dyn 28:425–440. doi:10.1007/s00382-006-0194-9

Wolfe AP, Miller GH, Olsen CA, Forman SL, Doran PT, Holmgren SU (2004) Geochronology of high latitude lake sediments. In: Pienitz R, Douglas MSV, Smol JP (eds) Long-term environmental change in Arctic and Antarctic Lakes. Kluwer Academic Publishers, Dordrecht, The Netherlands, pp 19–52

Yu Z, Walker KN, Evenson EB, Hajdas I (2008) Lateglacial and early Holocene climate oscillations in the Matanuska Valley, south-central Alaska. Quat Sci Rev 27:148–161. doi:10.1016/j.quascirev.2007.02.020